Journal of Solid State Chemistry 182 (2009) 2748–2755

Contents lists available at ScienceDirect

Journal of Solid State Chemistry

journal homepage: www.elsevier.com/locate/jssc

Displacive disorder and dielectric relaxation in the stoichiometric bismuth-containing pyrochlores, $Bi_2M^{III}NbO_7$ (M = In and Sc)

Yun Liu [a], Ray L. Withers [a,*], Hai Binh Nguyen [a], Kim Elliott [a], Qijun Ren [b], Zhanghai Chen [b]

[a] Research School of Chemistry, The Australian National University, Canberra, ACT 0200, Australia
[b] Surface Physics Laboratory and Physics Department, Fudan University, Shanghai 200433, China

ARTICLE INFO

Article history:
Received 25 March 2009
Received in revised form
15 June 2009
Accepted 4 July 2009
Available online 12 August 2009

Keywords:
A site stoichiometric
Bi-based pyrochlores
Displacive disorder
Dielectric relaxation
1-D dipoles
Electron diffraction

ABSTRACT

The structural disorder and temperature-dependent dielectric properties of two Bi-based niobate pyrochlore systems which have both previously been reported to occur at the ideal $Bi_2(M^{III}Nb^{V})O_7$ stoichiometry without any compositional disorder on the pyrochlore A site, namely the Bi_2InNbO_7 (BIN) and Bi_2ScNbO_7 (BSN) pyrochlore systems, have been carefully re-investigated. It is established that A site stoichiometric, Bi-based niobate pyrochlores can indeed exist. Electron diffraction is used to investigate the nature of the displacive disorder therein both at room temperature as well as at close to liquid nitrogen temperature. The characteristic structured diffuse scattering observed arises from β-cristobalite-like, 1-d correlated rotations and associated translations of chains of corner-connected $O'Bi_4$ tetrahedra. The temperature-dependent dielectric properties including the low temperature dielectric relaxation properties of these A site stoichiometric, Bi-based niobate pyrochlores are also reported as are the micro-Raman spectra thereof. The experimental results suggest that the dipoles as well as the glassy relaxation behaviour in these Bi-based pyrochlores are directly related to these β-cristobalite-like, correlated rotations of $\langle 110 \rangle$ chains of corner-connected $O'Bi_4$ tetrahedra.

1. Introduction

The $A_2B_2O_7$, or $B_2O_6.O'A_2$, cubic $Fd\bar{3}m$ ideal pyrochlore structure type can be described as being built out of two relatively weakly interacting, intergrown sub-structures, a B_2O_6 octahedral sub-structure and an $O'A_2$ tetrahedral sub-structure, of anti-cristobalite structure type (see e.g. Fig. 1a). Bismuth-based niobate pyrochlores, are inherently (chemically and) displacively disordered variants thereof (see e.g. Fig. 1b) which typically exhibit relatively high, room temperature dielectric permittivities (~70–200), low dielectric losses (~10^{-3}–10^{-4} in the MHz range) as well as relatively low sintering temperatures (~900–1000 °C) [1–5]. This combination of properties makes them rather useful as low temperature co-fired ceramic (LTCC) dielectric components for multilayer ceramic capacitor applications, particularly when taken in conjunction with the recently demonstrated electric field tuneability of these dielectric properties [6–8].

The composition of these bismuth-based niobate pyrochlores had traditionally been assumed to be fixed and of ideal stoichiometry $Bi_2M^{III}NbO_7$, or $M^{III}NbO_6.O'Bi_2$, and $Bi_2M^{II}_{2/3}Nb_{4/3}O_7$, or $M^{II}_{2/3}Nb_{4/3}O_6.O'Bi_2$ [1,2]. Recent careful phase analysis and structural studies have shown that this is not, in general, the case. $Bi_2Zn_{2/3}Nb_{4/3}O_7$, for example, has been shown not to be a true cubic pyrochlore at all but rather a monoclinic zirconolite [9]. Likewise, the true cubic pyrochlore phase in many such systems has recently been shown to often be a solid solution, significantly Bi-deficient with respect to the above traditional stoichiometries and to require the presence of nominally too small M^{2+} or M^{3+} cations on the A as well as the B sites of the ideal $A_2B_2O_7$ pyrochlore structure type (see e.g. [4,5,10–14]). They have thus recently been christened 'misplaced-displacive' cubic pyrochlores [10].

On cooling to low temperatures (~70–250 K), they typically exhibit an anomalous, frequency dispersive, step-like decrease in the real part of the dielectric permittivity along with a correlated, broad, frequency-dependent peak in the imaginary part of the dielectric permittivity [1–4,14–17] (see e.g. Fig. 2). Similar behaviour has recently also been reported for a non-Bi containing, ~$Ca_{1.47}Ti_{1.47}Nb_{1.04}O_7$ 'misplaced-displacive' cubic pyrochlore [18,19]. Such low temperature dielectric relaxation behaviour is strongly reminiscent of the behaviour of relaxor ferroelectrics [2–3,15–17] as well as of electric dipolar and quadrupolar glasses (such as e.g. $Rb_{1-x}(NH_4)_xH_2PO_4$ [2,20,21]). The low temperature peak in the imaginary part of the dielectric permittivity (at T_m) in the MHz region typically moves systematically to higher temperature upon increasing frequency (see Fig. 2). Indeed, its positioning (at room temperature) practically rules out the room temperature use of many of these

* Corresponding author.
E-mail address: withers@rsc.anu.edu.au (R.L. Withers).

0022-4596/$ - see front matter © 2009 Elsevier Inc. All rights reserved.
doi:10.1016/j.jssc.2009.07.007

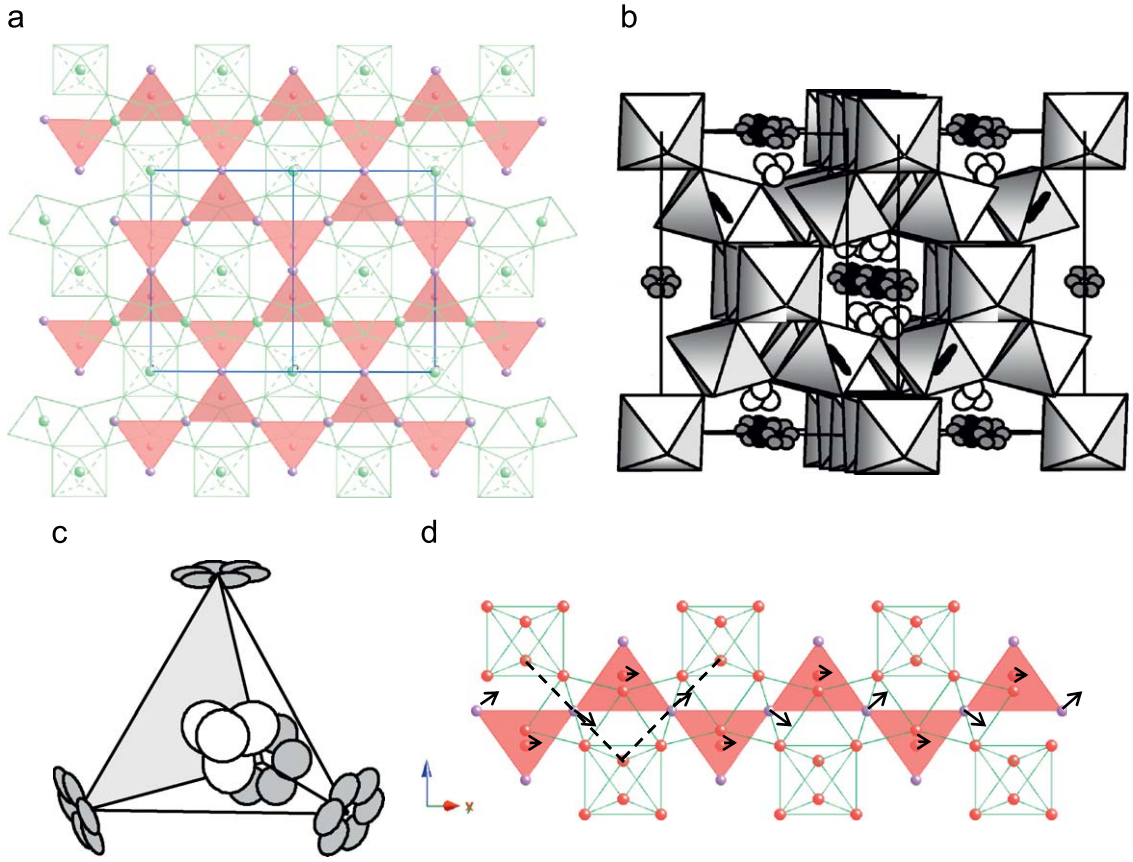

Fig. 1. (Colour online) The (a) O′A_2 tetrahedral framework sub-structure (the individual O′A_4 tetrahedra are shaded) and the intergrown B_2O_6 octahedral framework sub-structure (the individual BO_6 octahedra are outlined) of the ideal pyrochlore $A_2B_2O_7$ structure-type projected along a 〈110〉 direction. (b) The displacively disordered average structure of $Bi_{1.667}Mg_{0.70}Nb_{1.52}O_7$ projected along a close to 〈110〉 direction (see [9] for details). The corner-connected octahedral array represents the $(Mg_{0.24}Nb_{0.76})_2O_6$ octahedral sub-structure. The toroids of flat ellipsoids represent the six equivalent 96*h* *A* site positions of the O′$(Bi_{0.833}Mg_{0.11})_2$ sub-structure. The tetrahedral clusters of ellipsoids represent the four equivalent 32*e* site positions for the displaced O′ oxygens. (c) Shows an expanded view of one particular O′$(Bi_{0.833}Mg_{0.11})_4$ tetrahedron. (d) Shows the characteristic 1-d, *β*-cristobalite type displacive disorder of the O′A_2 sub-structure drawn relative to the surrounding B_2O_6 octahedral framework sub-structure. The tetrahedral edge rotation axes run along the projection direction.

Bi-based pyrochlores in the commercially important RF/MW frequency range [2]. It is therefore of some considerable importance, from both the fundamental as well as applied points of view, to be able to identify and understand the structural origin of the dipole moments as well as the glassy dielectric relaxation behaviour of these dipoles.

While the dipolar origin of the anomalous relaxation behaviour has yet to be clearly identified, it is apparent that the displacive disorder associated with the tetrahedral O′A_2 sub-structure (see e.g. Figs. 1b and c), and not simply the presence of a polarizable lone pair cation such as Bi^{3+} on the pyrochlore *A* site [18,19], is intimately involved [3,15–17]. The current prevailing view seems to be that the "…relaxation stem(s) from the (random) hopping of dynamically disordered *A* and O′ ions among (discrete but) closely spaced possible positions…" [17] (see e.g. Figs. 1b and c). (In this context, the recent DFT calculations on the displacively disordered $Bi_2Ti_2O_7$ pyrochlore suggesting the presence of multiple possible displacement sites and that the hopping is far from random [22] are interesting). Whether this displacive disorder (hopping) is inherent or induced by chemical disorder, in particular on the pyrochlore *A* site, however, is far from clear e.g. "…the partial substitution of Zn ions for Bi ions leads to more than one equivalent potential minima at the *A* sites and…to the dielectric relaxation…" [3]. The inherent displacive disorder in the pure Bi on *A* site, $Bi_2Ti_2O_7$ pyrochlore [22,23] shows that displacive disorder can certainly exist without chemical disorder on the O′A_2 sub-structure. Unfortunately, the method of synthesis of this $Bi_2Ti_2O_7$ pyrochlore rules out the preparation of a sufficiently dense sample to measure whether a low temperature dielectric relaxation also exists in $Bi_2Ti_2O_7$ [23] as a result of this inherent displacive disorder.

Given the recent discovery [10] that many, if not most, Bi-based niobate pyrochlores do not in fact form at the nominally ideal $Bi_2(M^{II}_{2/3}Nb^{5+}_{4/3})O_7$ or $Bi_2(M^{III}Nb^{5+})O_7$ pyrochlore type compositions [2] but rather form so-called 'misplaced-displacive' pyrochlore solid solutions with up to ~25% of the *A* site positions being occupied by nominally too small, typically *B* site cations [4,5,10,13,14,24,25], it might seem that the displacive disorder induced by the misplacement of the traditional *B* site cations onto the *A* sites (i.e. by chemical disorder) might be causally connected with the low temperature dielectric relaxation behaviour. If this were the case, however, the large amplitude displacive disorder and associated low temperature dielectric relaxation behaviour should not occur unless compositional disorder is present on the pyrochlore *A* site i.e. unless a cation other than Bi occupies the *A* site. It therefore becomes important to investigate the role of chemical disorder in the O′A_2 sub-structure on the displacive disorder and dielectric behaviour of these systems.

In this paper, we therefore investigate the structural disorder and low temperature dielectric properties of two particular Bi-based niobate pyrochlore systems which have both previously been reported to occur at the ideal $Bi_2(M^{III}Nb^{V})O_7$ stoichiometry without any compositional disorder on the pyrochlore *A* site, namely the Bi_2InNbO_7 (BIN) and Bi_2ScNbO_7 (BSN) pyrochlore

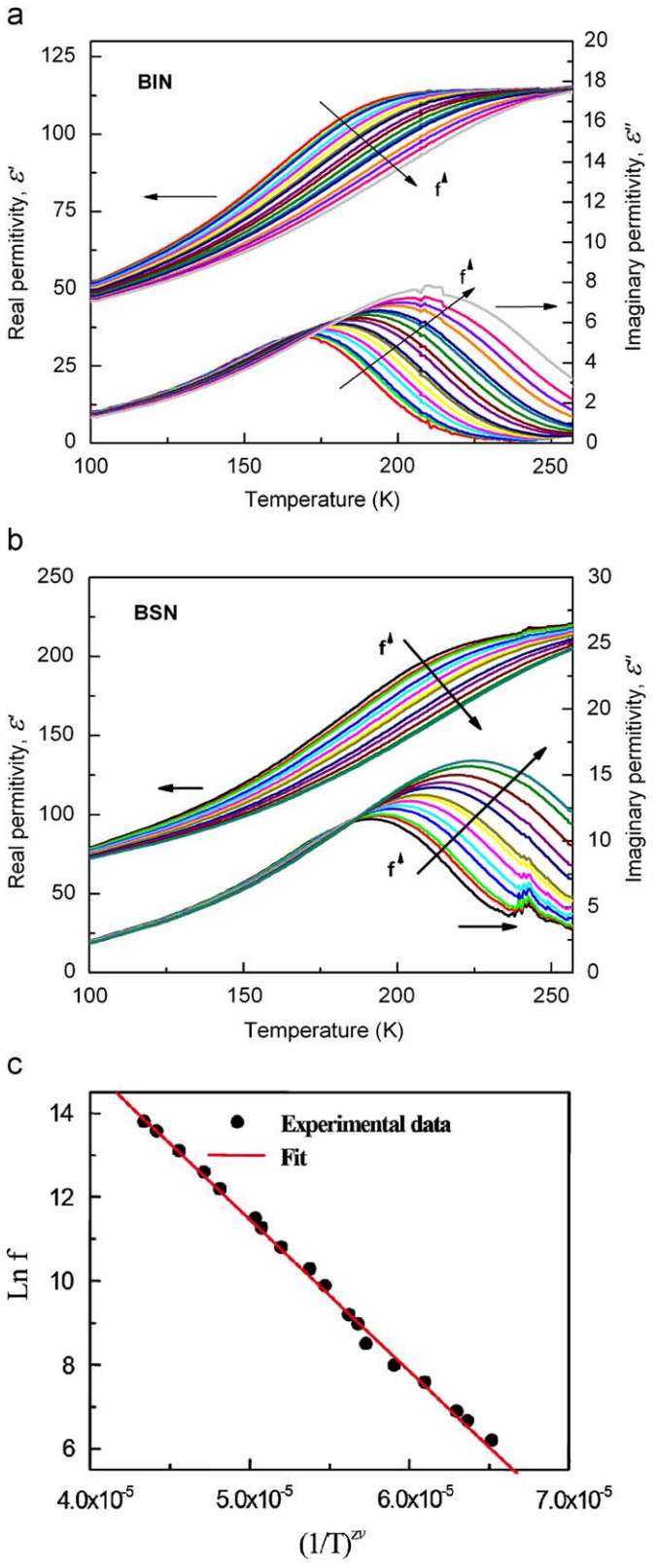

Fig. 2. The temperature-dependence of the real and imaginary parts of the dielectric permittivity of (a) BIN and (b) BSN at frequencies from 500 Hz to 1 MHz. (c) The best fit to the maximum in the dielectric loss as a function of frequency for the BIN sample using the relation $f = f_0 \exp -(T_{E_a}/T)^{z\nu}$, where $T_{E_a} = E_a/k$ and $z\nu = 1.9$.

systems [2]. The purpose is, firstly, to establish whether or not *A* site stoichiometric, Bi-based niobate pyrochlores can really exist; secondly, to use electron diffraction to investigate the nature of the displacive disorder therein and, thirdly, to re-investigate the dielectric relaxation properties of these *A* site stoichiometric, Bi-based niobate pyrochlores.

2. Experimental

2.1. Sample fabrication

Bi_2InNbO_7 (BIN) and Bi_2ScNbO_7 (BSN) at the ideal nominal compositions were both synthesized via solid state reaction. The starting materials used were high purity Bi_2O_3 (99.995%, Koch-Light), In_2O_3 (99.99%, Aldrich), Sc_2O_3 (99.99%, Hudson Lab.) and Nb_2O_5 (99.9+ %, Alfa) respectively. The appropriate oxides were initially homogeneously mixed in acetone for 30 min using an agate mortar, then calcined at 800 °C for one day in a Pt crucible followed by regrinding in acetone for a further 30 min. They were then pressed into pellets and annealed at 1050 °C for 2 days in the case of the BIN sample and at 1000 °C for 2 days in the case of the BSN sample.

2.2. X-ray powder diffraction

X-ray powder diffraction patterns of both samples were initially collected on a SIEMENS D-5000 diffractometer using Cu $K\alpha$ radiation. For higher resolution, powder XRD data were also obtained using a Guinier–Hägg focusing camera with Cu $K\alpha 1$ radiation. Silicon (NBS 640) was used as an internal standard for accurate determination of unit cell parameters, refined using the 'Unitcell' software package [26].

2.3. Electron probe microanalysis

Electron probe microanalysis (EPMA) was performed on the resultant samples in a JEOL 6400 scanning electron microscope (SEM) equipped with an Oxford Instruments light element EDS detector and Link ISIS SEMquant software. Quantitative EPMA analyses were carried out at 15 kV and 1 nA using $BiNbO_4$, Sc_2O_3 and $InNbO_4$ as internal calibration standards.

2.4. Electron diffraction

Grids suitable for transmission electron microscopy were prepared by crushing some of the samples in acetone and dispersing them onto lacey carbon coated grids. Electron diffraction patterns (EDPs) were obtained using a Philips EM 430 TEM operating at 300 kV. EDP's at close to liquid nitrogen temperature were obtained using a liquid nitrogen cold stage on the same Philips EM 430 TEM.

2.5. Dielectric property measurements

Pellets of measured relative density 7.80 and 6.60 g/cm^3 for the BIN and BSN samples respectively, corresponding to 97% and 90% of theoretical density as measured by Archimedes' method, were polished and coated with silver paste on both sides, followed by heat treatment at 550 °C to ensure good electrical contact. The dielectric properties of the pellets were then measured using a high-precision LCR metre (Agilent 4284A) and environmental boxes over the temperature range from liquid nitrogen to 260 K.

2.6. Raman spectroscopy

Temperature-dependent micro-Raman spectra were also collected from 77 K up to room temperature (293 K) using confocal

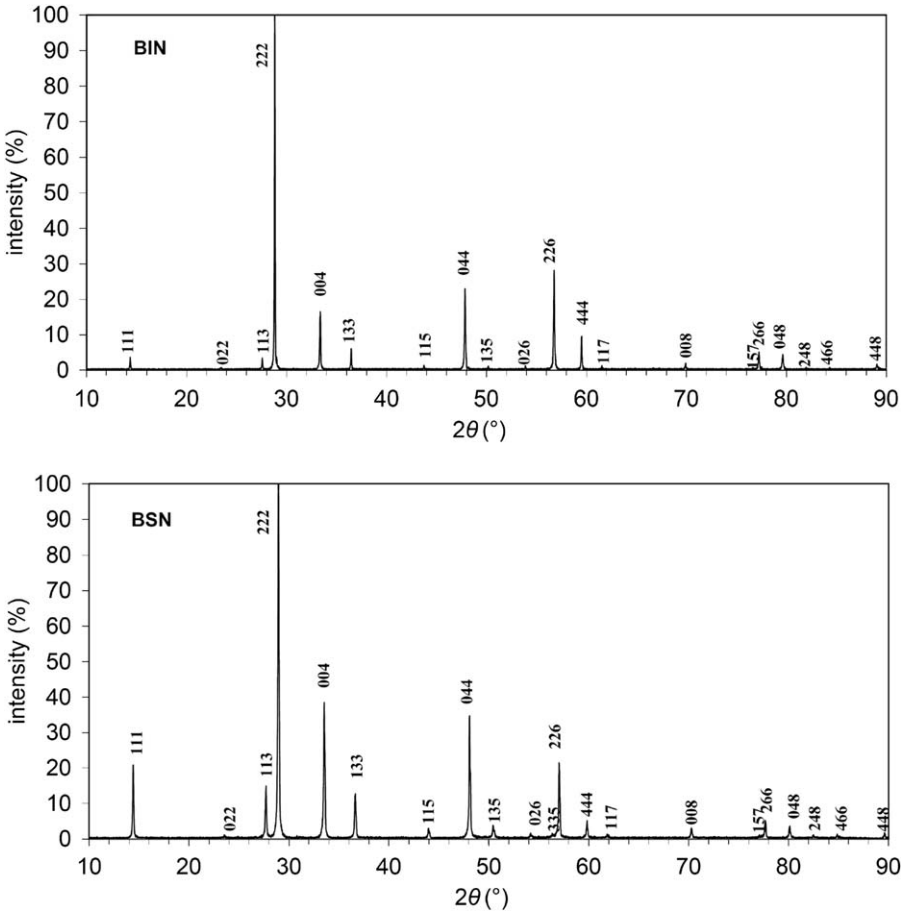

Fig. 3. XRD patterns of both BIN and BSN samples collected on a SIEMENS D-5000 diffractometer using Cu $K\alpha$ radiation.

micro-Raman spectroscopy (Jobin-Yvon HR800) in backscattering geometry. The excitation used a 632.8 nm line from a He–Ne laser. The laser power was ~10 W with a spot size ~1 μm. The backscattered light was dispersed using a 600 lines/mm grating and collected by a CCD array detector. This configuration allowed the recording of spectra with a spectral resolution of 1 cm^{-1}.

3. Results

Fig. 3 shows XRD patterns of both the BIN and BSN samples. No trace of an impurity phase could be found in either pattern. Rather, both samples were found to be single phase cubic pyrochlore to XRD, implying the nominal $Bi_2M^{III}NbO_7$ stoichiometry. The average structure of the BIN and BSN samples were indexed to the usual $Fd\bar{3}m$, fcc cubic pyrochlore unit cell giving $a = 10.792(2)$ Å in the case of BIN and $a = 10.660(9)$ Å in the case of BSN. The presence of weak reflections forbidden for the ideal pyrochlore structure type, such as the 248 reflection, in both cases is indicative of inherent displacive disorder in the O′A_2 sub-structure (as pointed out by Vanderah and colleagues [10,12,13]).

In order to confirm the nominal Bi_2MNbO_7 stoichiometry, the as-synthesized samples were further investigated by quantitative EPMA to check for homogeneity and composition, using $BiNbO_4$, Sc_2O_3 and $InNbO_4$ as calibration standards. Note that the typical accuracy of quantitative EPMA using appropriate calibration standards is accepted to be $\sim\pm 2\%$ relative (see e.g. [27]). In the case of BIN, the sample was found to be homogeneous and single phase of average composition $Bi_{1.98(2)}In_{0.99(2)}Nb_{1.01(2)}O_7$ (normalized to seven oxygens). In the case of BSN, the sample was again found to be homogeneous and single phase of average composition $Bi_{1.99(1)}Sc_{0.96(1)}Nb_{1.03(1)}O_7$. Both EPMA determined compositions are thus in agreement (within error) to the nominal starting stoichiometries. The quoted error bars represent the standard deviation from 20 separate spot analyses used to obtain the quoted average compositions. Thus the possibility of *A*-site stoichiometric, $Bi_2M^{3+}NbO_7$ niobate pyrochlores, with Bi only occupying the *A* sites, is established.

In order to investigate disorder in these samples, electron diffraction was carried out both at room temperature as well as at close to liquid nitrogen temperature (well below the peak in the imaginary permittivity at T_m, see Fig. 2) searching for evidence of structured diffuse scattering characteristic of chemical and/or displacive disorder. Fig. 4 shows typical (a) ⟨1,−1,0⟩, (b) ⟨−2,2,1⟩, (c) ⟨−3,6,−1⟩ and (d) ⟨5,1,−2⟩ zone axis electron diffraction patterns (EDPs) of BSN at room temperature while Fig. 5 shows (a) ⟨−1,−1,10⟩ and (b) ⟨−5,3,2⟩ zone axis EDPs of BSN at close to liquid nitrogen temperature. Essentially identical EDP's were found for BIN (see also [25,28]). Highly structured diffuse streaking is present in each EDP both above and below T_m, always running along a ⟨*h*,−*h*, *l*⟩* direction of reciprocal space orthogonal to one of the six ⟨110⟩ directions of the underlying average structure e.g. in Fig. 4b, diffuse streaking running along the [12,8,8]*, [8,12,−8]* and [2,−2,8]* directions of reciprocal space orthogonal to the [0,1,−1], [101] and [110] directions of real space respectively is clearly apparent while, in Fig. 4d, diffuse streaking running along the [3,−5,5]*, [1,−7,−1]* and [155]* directions of reciprocal space orthogonal to the [011], [101] and [0,1,−1] directions of real space is likewise clearly apparent etc.

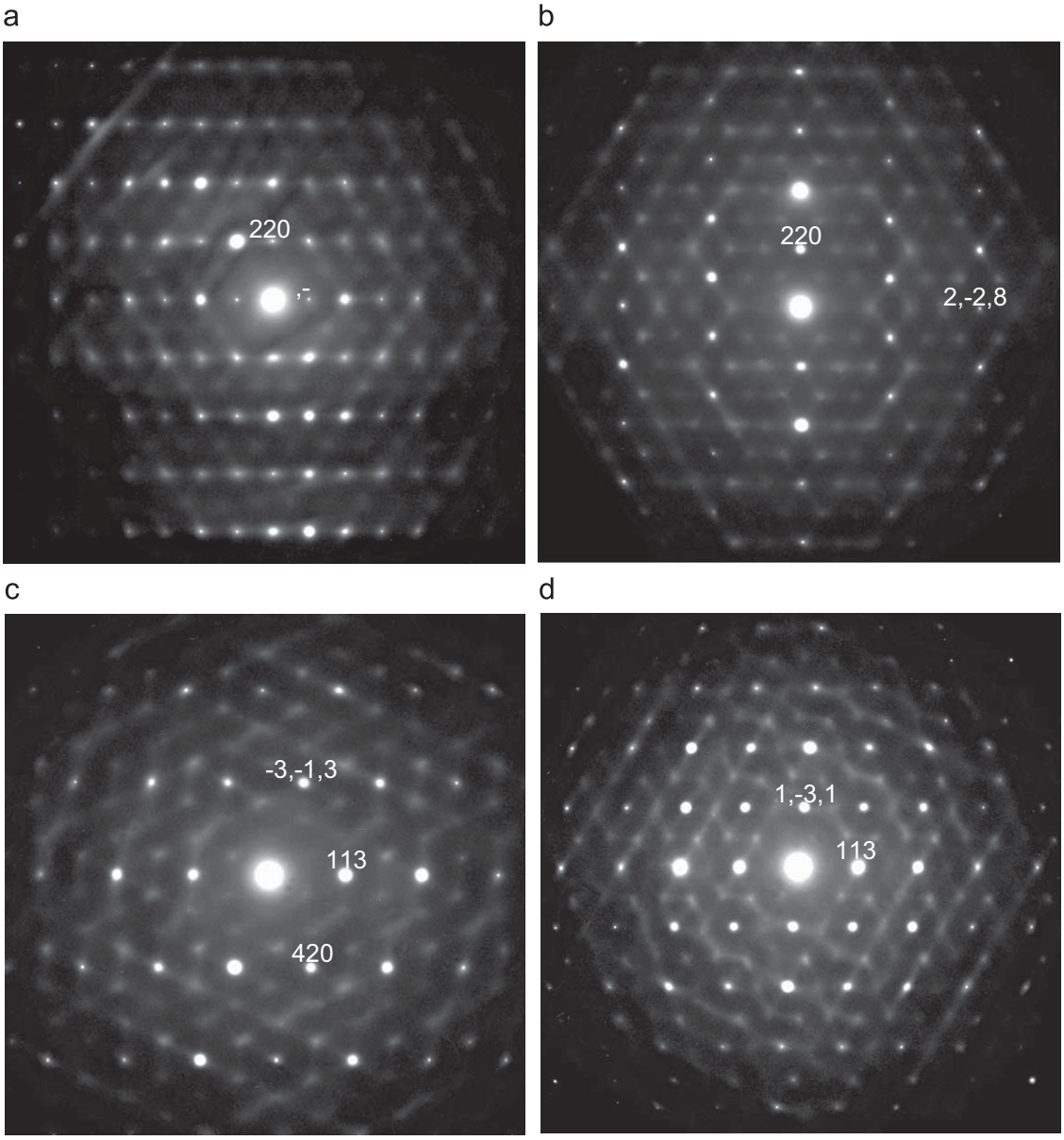

Fig. 4. Typical (a) ⟨1,−1,0⟩, (b) ⟨−2,2,1⟩, (c) ⟨−3,6,−1⟩ and (d) ⟨5,1,−2⟩ zone axis electron diffraction patterns (EDPs) of BSN.

Such diffuse streaking collectively takes the form of well-defined {110}* sheets of diffuse intensity orthogonal to the six ⟨110⟩ directions of the underlying average structure. Essentially identical structured diffuse scattering has already been reported to be characteristic of BIN [25,28] as well as the close to *A* site stoichiometric $Bi_2Ru_2O_{7-\delta}$ [29] and $(Bi_{1.89}Fe_{0.11})(Fe_{1.05}Nb_{0.95})O_{6.95}$ (BFN) [25] pyrochlores. (Related but subtly different diffuse scattering has also been found in the more *A* site compositionally disordered $(Bi_{1.65}Ni_{0.25}\square_{0.10})(Ni_{0.50}Nb_{1.50})O_7$ (BNN) and $(Bi_{1.67}Mg_{0.17}\square_{0.16})(Ni_{0.47}Nb_{1.53})O_7$ (BMN) samples [5]). The transverse polarized [29] nature of the characteristic observed structured diffuse distribution requires that the displacements responsible are both correlated as well as directed along the ⟨110⟩ directions without any correlation from one such ⟨110⟩ column to the next in the perpendicular direction as shown in Fig. 1d. Taken together with the diagnostic characteristic 'extinction condition' whereby the $\langle hkl\rangle^* \pm \varepsilon\langle h,-h,l\rangle^*$ sheets of diffuse intensity perpendicular to ⟨110⟩ are observed only when $h+k=4J$, J an integer, the observed diffuse scattering can only arise from β-cristobalite-like, correlated rotations and associated translations of chains of corner-connected $O'Bi_4$ tetrahedra, as shown in Fig. 1d. Note that from the diffraction point of view, these polar displacive modes of distortion could be either static or dynamic in nature.

The superposition of all such correlated chain rotation modes gives rise to an instantaneous real space distribution (see e.g. [29, Fig. 4b]) that is consistent not only with the observed structured diffuse intensity but also with the refined 'disordered' average structures of such Bi-pyrochlores (see e.g. Fig. 1b). In particular, it gives rise to strongly correlated O′ and Bi displacements, to a flat disc-like region of Bi occupancy perpendicular to the local O′–Bi–O′ axis as well as individual $O'Bi_4$ tetrahedra that are tightly constrained and rather closer to an ideal tetrahedron than the average structure might imply (see [29]). Note that the latter result suggests that "…the spin-ice rules found in complex Bi-based pyrochlores, where two-long and two-short bonds are found in each tetrahedron of $O'Bi_4$…" [22] and first proposed by Seshadri [30] in the context of ice are unlikely to be applicable in

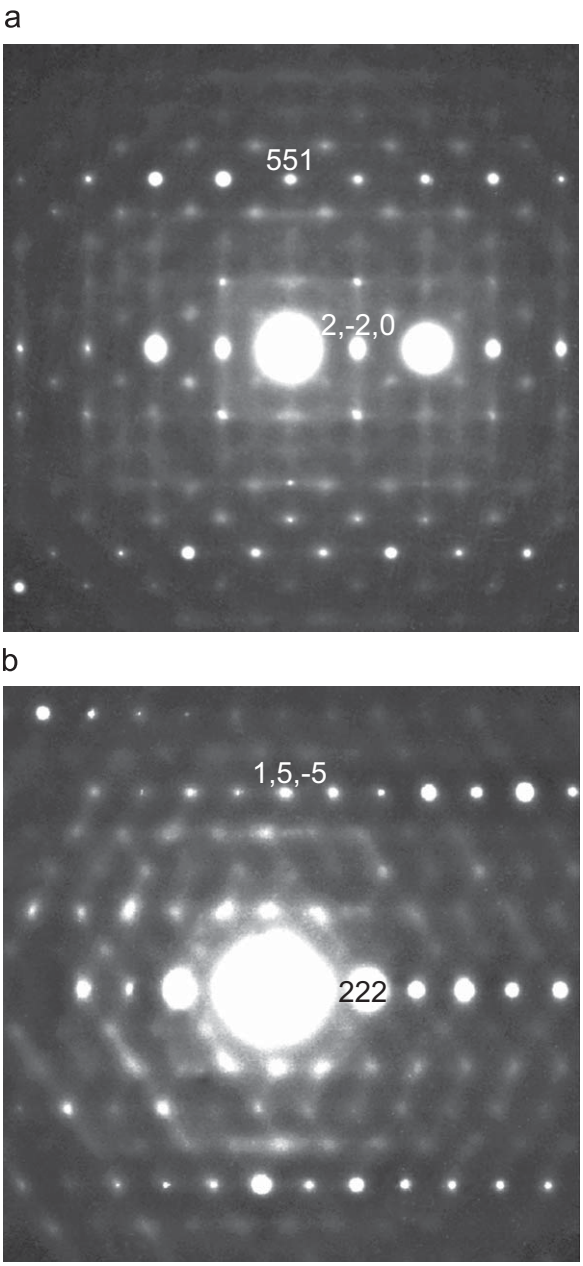

Fig. 5. Typical (a) ⟨−1,−1,10⟩ and (b) ⟨−5,3,2⟩ zone axis EDPs of BSN at close to liquid nitrogen temperature.

the case of displacively disordered (but non-chemically disordered) Bi-pyrochlores.

Note that the strongly anisotropic Bi distribution implied by correlated chain rotation modes and the observed diffuse distribution (see Figs. 4 and 5; see also [29]) is typically modelled in conventional powder diffraction analyses via split-site models around the ideal pyrochlore *A* site position as have commonly been reported (e.g. [4,12–14,23–25,28,31,32]). Usually this is modelled in terms of a single disordered site, typically either the 96*g* or 96*h* site. Various authors (see e.g. [4,23,24,32]), however, have pointed out that these two sites are virtually indistinguishable from the refinement point of view. Indeed, the recent DFT based investigation of the displacively disordered $Bi_2Ti_2O_7$ pyrochlore predicted occupancy of 96*g*, 96*h* as well as 192*i* sites [22]. Such results suggest that there may be no discrete disordered sites at all but rather an essentially continuous scattering density around the ideal pyrochlore *A* site position [32]. Such a viewpoint comes very close to the disordered *β*-cristobalite type model (see [29]).

It is most important to note that the *β*-cristobalite-like, correlated chain rotation modes required by the observed diffuse distribution involve rotation as well as rigid body translation of a nominally +4 charged $O'Bi_2$ column of tetrahedra along a ⟨110⟩ direction relative to the nominally −4 charged $M^{3+}Nb^{5+}O_6$ octahedral sub-structure (see Fig. 1b), thus leading to a net dipole moment along the relevant ⟨110⟩ direction. The polyhedral connectivity of the constituent $O'Bi_4$ tetrahedra in conjunction with the fact that the tetrahedral rotation is around a tetrahedral edge and not through the centre of the tetrahedron means that there need be no correlation in the sense of the rotation (and hence in the sign of the corresponding dipole moment) from one ⟨110⟩ chain to a neighbouring chain. The length in real space of these inherently 1-d dipolar chains (in essence 1-d polar nanoregions, PNR's) must be reasonably long to be compatible with the sharpness of the {110} sheets of diffuse intensity in reciprocal space (see Figs. 4 and 5).

The fact that the observed structured diffuse distribution takes the same form both above and below the peak in the imaginary part of the dielectric permittivity (see Figs. 4 and 5) does not mean that these 1-d PNR's are unrelated to the observed relaxor dielectric behaviour, in particular to the peak in the imaginary part of the dielectric permittivity at T_m (see Fig. 2). Essentially identical behaviour, for example, has been observed in the case of the $Ba(Ti_{1-x}Sn_x)O_3$ and $Ba(Ti_{1-x}Zr_x)O_3$, for $x \geq 0.1$, relaxor ferroelectric systems [33] and, more recently, in the case of a PLZT(7.0/60/40) sample close to the morphotropic phase boundary therein [34]. In each of these cases, the observed structured diffuse scattering arises from similar 1-d PNR's that are known to be directly related to the relaxor ferroelectric properties of the materials. The observed diffuse phase transition in these cases can thus only be attributed to a dynamic freezing or glass-like transition involving the slowing down of the dipolar dynamics of the 1-d PNR's [35] implied by the existence of the structured diffuse distribution [33–35].

The observed structured diffuse distribution implies that 1-d PNR's of the type shown in Fig. 1d exist along all six ⟨110⟩ directions. As shown by the example of SiO_2-cristobalite itself [36–38], it is possible for such a system to undergo a coherent structural phase transition on cooling i.e. for a particular RUM mode to condense out. Such a transition, however, usually requires the metric symmetry of the structure to be able to change in response. It is proposed that the rigidity of the $M^{III}NbO_6$ framework sub-structure in the case of BIN and BSN prevents strain distortion of the $O'Bi_2$ sub-structure itself and hence transverse correlation from one 1-d PNR to the next thereby giving rise to the glassy dielectric relaxation behaviour at low temperature and preventing the onset of long range ferroelectric ordering, even at the lowest possible temperatures. We suggest these intrinsically very low energy, correlated, chain rotation modes (analogous to the so-called rigid unit mode (RUM) modes of *β*-cristobalite [36–38]) provide an important key to understanding the structural origin of the dipoles as well as the glassy relaxation behaviour of Bi-based niobate pyrochlores.

While the low temperature dielectric properties of BIN and BSN have previously been reported [2], they have not been reported for BIN and BSN samples that have been explicitly shown to have the ideal Bi_2MNbO_7 stoichiometry. Fig. 2 shows the measured temperature-dependent real and imaginary parts of the dielectric permittivity of the BIN and BSN samples as a function of applied frequency from 500 Hz up to 1 MHz (a for BIN, b for BSN). The real and imaginary parts of the dielectric permittivity of both BIN and BSN exhibit very similar temperature-dependent dielectric relaxation behaviour to other non-stoichiometric Bi-based

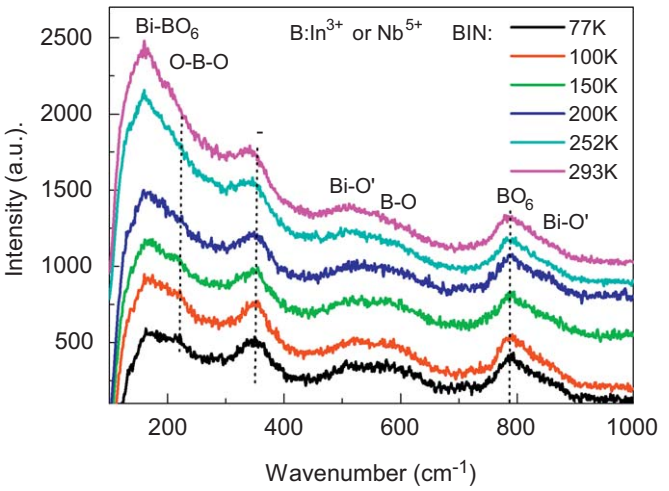

Fig. 6. The temperature dependent micro-Raman spectra of the BIN sample collected from 77 to 300 K.

pyrochlores e.g. the temperature (T_m) at which the dielectric loss peaks shifts systematically to higher temperature as the measuring frequency increases while the magnitude of the dielectric loss at this peak, as well as its temperature-dependent width, also increase systematically with increasing frequency [2,4,10,14–17].

Temperature-dependent micro-Raman spectra were also collected from 77 K up to room temperature (293 K) looking in particular for any evidence of some sort of structural phase transition in the vicinity of the peak in the imaginary part of the dielectric permittivity (see Fig. 2). Fig. 6 shows the measured micro-Raman spectra of the BIN sample from 77 K up to 293 K. The mode assignments follow those given in McCauley [39]. Note that the Bi–O stretch band at $\sim$350 cm^{-1} as well as the O–Bi–O band at $\sim$220 cm^{-1} appear to shift slightly in frequency as well as to gain some oscillator strength on cooling to low temperature. While there are some subtle shifts like this in the frequency and strength of the observed modes on cooling, there is clearly no evidence in the Raman spectra for any well-defined 'phase transition', in agreement with the observed temperature-dependent electron diffraction behaviour described above.

4. Discussion

Despite similarities, an important difference in the dielectric relaxation behaviour of the *A* site stoichiometric, BIN and BSN, pyrochlores relative to that of the non-stoichiometric Bi-based pyrochlores is that the peak in the imaginary part of the dielectric permittivity as a function of frequency is shifted to higher temperatures in the cases of BIN and BSN e.g. T_m at 1 MHz = 225 K for BSN and 210 K for BIN but only 133 K for BNN [14], 125 K for BFN [4], 114 K for BMN [14] and $\sim$110 K for BZN [17]. This is important in the context of the magnitude of the room temperature dielectric loss at RF/MW frequencies.

When the frequency dependence of the peak positions in the dielectric loss curves for BIN and BSN are modelled using the standard Arrhenius equation, completely unrealistic values are obtained e.g. an activation energy $E_a \sim 0.559$ eV (corresponding to a temperature of $\sim$6481 K) and an attempt jump, or freezing, frequency $f_0 \sim 2.05 \times 10^{20}$ Hz in the case of BIN, significantly higher than the freezing frequency of both ionic lattice vibrations ($\sim 10^{13}$ Hz) as well as free electron vibrations ($\sim 10^{16}$ Hz). Fitting using the Vogel–Fulcher equation gave no improvement. Following Cann et al. [2], the observed data were finally fitted via the relation $f = f_0 \exp(-T_{Ea}/T)^{zv}$, where $T_{E_a} = E_a/k$ and zv is a so-called dynamic scaling exponent [21,37] found to be $\sim$2. Rather more reasonable activation energies, E_a, of 0.071 (0.072) eV and attempt jump frequencies of 6.48 (6.34) THz were then obtained for BSN and (BIN) respectively. Whether these particular values have any real physical meaning, however, is not at all clear.

As stated above, it is proposed that the intrinsically very low energy, correlated, chain rotation modes implied by the observed structured diffuse distribution and shown in Fig. 1d provide an important key to understanding the structural origin of the dipoles as well as the glassy relaxation behaviour of these Bi-based pyrochlores. The near ubiquitous presence of essentially the same highly structured diffuse distribution in so many bi-pyrochlores [5,25,28,29] supports this contention. At the very least, it means that the (random) hopping model [3,15–17] is quite untenable. It also strongly suggests that there is no direct, or causal, link between the chemical disorder and the existence of the dipole moments. In the case of β-cristobalite itself, it is known that there exist numerous very low frequency RUM modes (see e.g. [36, Fig. 2]) which give rise to a very similar structured diffuse distribution as that shown in Figs. 4 and 5 and that the low frequency dynamics of the β-phase are very similar to those found in network glasses [36–38]. In the case of the Bi-pyrochlores, it is clear that there also exist numerous very low, if not zero, frequency RUM-type modes.

The intergrowth of the octahedral and β-cristobalite-like tetrahedral sub-structures in Bi-pyrochlores (see Fig. 1) not only differentiates them from β-cristobalite itself, it also constrains the overall metric symmetry to remain cubic and hence prevents the onset of long range ferroelectric order. The 'phase transition' represented by the low temperature, frequency-dependent peak in the dielectric loss (see Fig. 2) is thus not a conventional phase transition (as is clear from the electron diffraction data shown in Figs. 4 and 5 as well as the temperature-dependent micro-Raman data of Fig. 6) but rather a dynamic freezing or glass-like transition involving the slowing down of the 1-d dipolar dynamics of the PNR's.

Acknowledgment

The authors (YL, RLW and BN) acknowledge financial support from the Australian Research Council (ARC) in the form of ARC Discovery Grants.

References

[1] G.I. Golovshchikova, V.A. Isupov, A.G. Tutov, I.E. Mylnikova, P.A. Nikitina, O.I. Tulinova, Sov. Phys. Solid State 14 (1973) 2539.
[2] D.P. Cann, C.A. Randall, T.R. Shrout, Solid State Commun. 100 (1996) 529.
[3] C. Ahn, Z. Yu, H.J. Youn, C.A. Randall, A.S. Bhalla, L.E. Cross, J. Nino, M. Lanagan, Appl. Phys. Lett. 80 (2002) 4807.
[4] M.W. Lufaso, T.A. Vanderah, I.M. Pazos, I. Levin, R.S. Roth, J.C. Nino, V. Provenzano, P.K. Schenck, J. Solid State Chem. 179 (2006) 3900.
[5] B. Nguyen, Y. Liu, R.L. Withers, J. Solid State Chem. 180 (2007) 549.
[6] W. Ren, S. Trolier-McKinstry, C.A. Randall, T.R. Shrout, J. Appl. Phys. 89 (2001) 767.
[7] J.Y. Kim, D. Kim, H.S. Jung, K.S. Hong, J. Appl. Phys. 44 (2005) 6648.
[8] J. Lu, S. Stemmer, Appl. Phys. Lett. 83 (2003) 2411.
[9] I. Levin, T.G. Amos, J.C. Nino, T.A. Vanderah, I.M. Reaney, C.A. Randall, M.T. Lanagan, J. Mater. Res. 17 (2002) 1406.
[10] T.A. Vanderah, I. Levin, M.W. Lufaso, Eur. J. Inorg. Chem. (2005) 2895.
[11] M. Valant, D. Suvorov, J. Am. Ceram. Soc. 88 (2005) 2540.
[12] T.A. Vanderah, T. Siegrist, M.W. Lufaso, M.C. Yeager, R.S. Roth, J.C. Nino, S. Yates, Eur. J. Inorg. Chem. (2006) 4908.
[13] I. Levin, T.G. Amos, J.C. Nino, T.A. Vanderah, C.A. Randall, M.T. Lanagan, J. Solid State Chem. 168 (2002) 69.
[14] H.B. Nguyen, L. Norén, Y. Liu, et al., J. Solid State Chem. 180 (2007) 2558.
[15] J.C. Nino, M.T. Lanagan, C.A. Randall, J. Appl. Phys. 89 (2001) 4512.
[16] J.C. Nino, M.T. Lanagan, C.A. Randall, S. Kamba, Appl. Phys. Lett. 81 (2002) 4404.

[17] S. Kamba, V. Porokhonsky, A. Pashkin, et al., Phys. Rev. B 66 (2002) 054106.
[18] B. Nguyen, Y. Liu, R.L. Withers, Solid State Commun. 145 (2008) 72.
[19] R.S. Roth, T.A. Vanderah, P. Bordet, et al., J. Solid State Chem. 181 (2008) 406.
[20] E. Courtens, Phys. Rev. Lett. 52 (1984) 69.
[21] J.A. Mydosh, Spin Glasses: An Experimental Introduction, Taylor & Francis, London, 1993.
[22] B.B. Hinojosa, J.C. Nino, A. Asthgari, Phys. Rev. B 77 (2008) 104123.
[23] A.L. Hector, S.B. Wiggin, J. Solid State Chem. 179 (2006) 2495.
[24] R.L. Withers, T.R. Welberry, A.K. Larsson, et al., J. Solid State Chem. 177 (2004) 231.
[25] W. Somphon, V. Ting, Y. Liu, R.L. Withers, Q. Zhou, B.J. Kennedy, J. Solid State Chem. 179 (2006) 2495.
[26] B. Noläng, Inst. Materialkemi, Ångströmlaboratoriet, Box 538, S-751 21 Uppsala, Sweden.
[27] D. Newbury, R. Marinenko, J. Armstrong, J. Small, E. Steel, Microsc. Microanal. 9 (Suppl. 2) (2003) 528.
[28] Q. Zhou, B.J. Kennedy, V. Ting, et al., J. Solid State Chem. 178 (2005) 1575.
[29] A.L. Goodwin, R.L. Withers, H.-B. Nguyen, J. Phys. Condens. Matter 19 (2007) 335216.
[30] R. Seshadri, Solid State Sci. 8 (2006) 259.
[31] B. Melot, E. Rodriguez, Th. Proffen, M.A. Hayward, R. Seshadri, Mater. Res. Bull. 41 (2006) 961.
[32] M. Avdeev, M.K. Haas, J.D. Jorgensen, R.J. Cava, J. Solid State Chem. 169 (2002) 24.
[33] Y. Liu, R.L. Withers, X. Wei, J.D. Fitz Gerald, J. Solid State Chem. 180 (2007) 858.
[34] R.L. Withers, Y. Liu, T.R. Welberry, J. Solid State Chem. 182 (2009) 348.
[35] V. Bovtun, J. Petzelt, V. Porokhonsky, et al., J. Eur. Ceram. Soc. 21 (2001) 1307.
[36] I.P. Swainson, M.T. Dove, Phys. Rev. Lett. 71 (1993) 193.
[37] S.A. Wells, M.T. Dove, M.G. Tucker, K. Trachenko, J. Phys. Condens. Matter 14 (2002) 4645.
[38] I.P. Swainson, M.T. Dove, J. Phys. Condens. Matter 7 (1995) 1771.
[39] R.A. McCauley, J. Opt. Soc. Am. 63 (1973) 721.